

Chemically Modified mRNAs for Highly Efficient Protein Expression in Mammalian Cells

Published as part of the ACS Chemical Biology Young Investigators virtual special issue

Abhishek Aditham,[△] Hailing Shi,[△] Jianting Guo, Hu Zeng, Yiming Zhou, Sarah Dunn Wade, Jiahao Huang, Jia Liu, and Xiao Wang*



Cite This: *ACS Chem. Biol.* 2022, 17, 3352–3366



Read Online

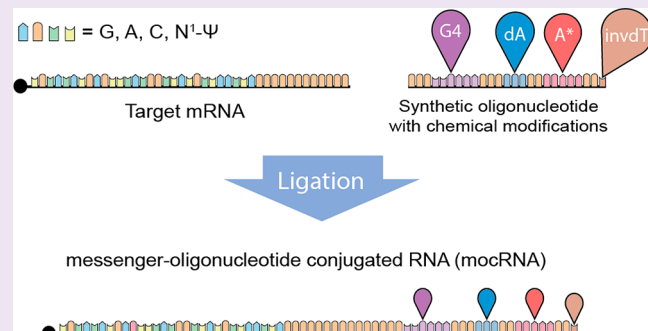
ACCESS |

Metrics & More

Article Recommendations

Supporting Information

ABSTRACT: mRNA has recently been established as a new class of therapeutics, due to its programmability and ability to produce proteins of interest rapidly *in vivo*. Despite its demonstrated utility, mRNA as a protein expression platform remains limited by its translational capacity and RNA stability. Here, we introduce messenger-oligonucleotide conjugated RNAs (mocRNAs) to enable site-specific, robust, and modularized encoding of chemical modifications for highly efficient and stable protein expression. In mocRNA constructs, chemically synthesized oligonucleotides are ligated to the 3' terminus of mRNA substrates to protect poly(A) tails from degradation, without compromising their potency in stimulating translation. As a proof-of-concept, mocRNAs modified by deadenylase-resistant oligonucleotides result in augmented protein production by factors of 2–4 in human HeLa cells and by 10-fold in primary rat cortical neuronal cultures. By directly linking enzymatic and organic synthesis of mRNA, we envision that the mocRNA design will open new avenues to expand the chemical space and translational capacity of RNA-based vectors in basic research and therapeutic applications.



Downloaded via 71.233.150.153 on March 3, 2023 at 08:06:41 (UTC).
 See https://pubs.acs.org/sharingguidelines for options on how to legitimately share published articles.

INTRODUCTION

As evidenced by recent clinical trials and approvals of messenger RNA (mRNA) vaccines for SARS-CoV-2,^{1,2} mRNA is an emerging and promising alternative to conventional protein-based drugs. This is mainly due to its programmability, rapid production of proteins *in vivo*, relatively low-cost manufacturing, and potential scalability to produce multiple proteins simultaneously.^{3–5} However, while mRNAs have been shown to robustly generate therapeutic proteins *in vivo*,^{3,6–8} their relatively short lifetimes may limit their clinical applications where high quantities of protein production are required.^{3,9} Depending on the intended functions of therapeutic proteins, the dosage and treatment duration of mRNA drugs could vary by orders of magnitude. For vaccines, the expression of nanogram to microgram ranges of an antigen could be sufficient for eliciting an immune response.³ However, for growth factors, hormones, or antibodies, the therapeutic dose could range from micrograms to milligrams, or potentially up to gram quantities of protein.³ Simply scaling up mRNA quantity to achieve high protein production may lead to dose-dependent toxicity, due to the innate immune stimulation inherent to transfection of mRNA.³ This combination of factors drives the need for engineering mRNA vectors to boost transgenic protein production without

increasing dosage, particularly through enhancements to mRNA lifetime and/or translational efficiency.

Chemical modification is an effective way to enhance the performance of mRNA vectors. Exogenous mRNAs prepared by *in vitro* transcription (IVT) consisting of “unmodified” adenosine (A), guanosine (G), cytidine (C), and uridine (U) strongly trigger innate immune toxicity that suppresses protein expression.^{10–12} Incorporation of modified U derivatives, such as pseudouridine and N¹-methylpseudouridine, has been widely used to increase translation, specifically by decreasing innate immune toxicity through blocking Toll-like receptor recognition.^{10–14} However, this strategy currently limits the chemical space of mRNA modifications available for incorporation, as many modified NTPs are not tolerated by RNA polymerases or ribosomal machinery. Moreover, certain chemical modifications in the protein-coding region of mRNAs could potentially cause impaired translation.^{14–16} An alter-

Received: July 22, 2021

Accepted: December 3, 2021

Published: January 7, 2022



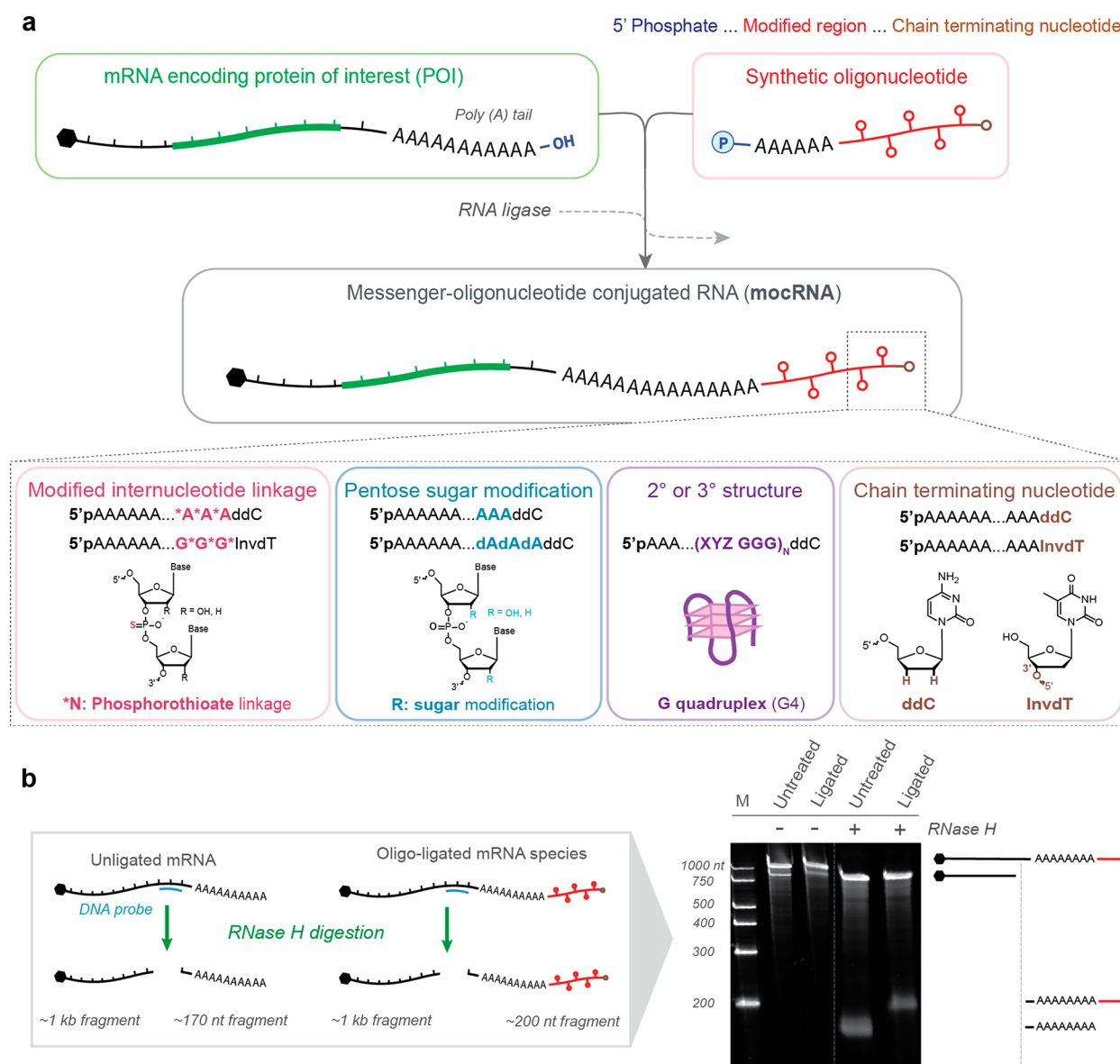


Figure 1. Synthetic strategies of messenger-oligonucleotide conjugated RNAs (mocRNAs). (a) mocRNA synthesis schematic, with an overview of chemical modifications and structures of synthetic oligos used for ligations. Chemically synthesized oligos with defined compositions were ligated to the 3' end of humanized Monster Green Fluorescent Protein (GFP) mRNAs containing a template-encoded 60 nt poly(A) sequence (GFP-60A), to produce translatable mocRNAs. (b) Schematics of the RNase H assay used to quantify ligation reaction efficiency of mocRNAs. Oligonucleotides used for ligations were 30 nt. DNA probes (blue) target the 3' UTR of mRNA such that the 5' end of the probe is 106 nt upstream of the poly(A) tail. This generates a 5' mRNA fragment (824 nt) and a 3' mRNA fragment (166 nt including the 60 nt poly(A) tail for unligated mRNA; ~200 nt for ligated mRNA). The 3' cleavage product displays a band shift on a denaturing gel upon ligation. M, Marker; Century-Plus RNA Markers.

native strategy to increase mRNA stability without modifying the coding region is to selectively incorporate modified NTPs during enzymatic extension of the mRNA poly(A) tail, which is particularly sensitive to exonucleases in the cell.^{17,18} While promising, this strategy relies on poly(A) polymerases, which again face limited chemical repertoires, variable efficiencies of enzymatic incorporation, and generation of a variable distribution of poly(A) tail lengths.¹⁸

To overcome the aforementioned limitations, we developed a ligation-based strategy to efficiently construct messenger-oligonucleotide conjugated RNAs (mocRNAs), an mRNA-based expression system with augmented protein production capacity. In this approach, synthetic oligonucleotides (oligos) are ligated with the 3' ends of mRNAs containing template-

encoded poly(A) tails (Figure 1a,b). This enables precise and modularized encoding of chemical modifications into RNA vectors, which is not possible using RNA polymerase-mediated incorporation. Shortening of the poly(A) tail is identified as a critical step in cellular mRNA decay, and the poly(A) tail is indispensable for cap-dependent translation.^{19,20} Thus, as a proof-of-concept of the mocRNA system, we designed and tested various nuclease-resistant motifs²¹ in synthetic oligonucleotides to protect poly(A) tails, which demonstrated superior protein expression in comparison with alternative variants of mRNA vectors.

Table 1. List and Sequences of Oligonucleotides Used for mocRNA Syntheses^a

| Modified oligonucleotide name | Sequence |
|-------------------------------|---|
| 29rA_ddC | /SPhos/rArArA rArArA rArArA rArArA rArArA rArArA rArArA rArArA rArArA rArArA/3ddC/ |
| 3xSrA_ddC | /SPhos/rArArA rArArA rArArA rArArA rArArA rArArA rArArA rArArA rArArA* rA* rA* rA* rA* /3ddC/ |
| 3xSrA_InvdT | /SPhos/rArArA rArArA rArArA rArArA rArArA rArArA rArArA rArArA rArArA* rA* rA* /3InvdT/ |
| 3xSrG_InvdT | /SPhos/rArArA rArArA rArArA rArArA rArArA rArArA rArArA rArArA rArArG* rG* rG* /3InvdT/ |
| 6xSr(AG) | /SPhos/rArArA rArArA rArArA rArArA rArArA rArArA rArArA rArArA rArArA* rA* rA* rG* rG* /3InvdT/ |
| 3xdA_ddC | /SPhos/rArArA rArArA rArArA rArArA rArArA rArArA rArArA rArArA rArAA AA/3ddC/ |
| 23xdA_ddC | /SPhos/rArArA rArArA AAA AAA AAA AAA AAA AAA AA/3ddC/ |
| G4_telo_DNA_GtoC | /SPhos/rArArA rArArA TAC CCT TAC CCT TAC CC/3ddC/ |
| G4_telo_DNA_WT | /SPhos/rArArA rArArA TAG GGT TAG GGT TAG GG/3ddC/ |
| G4_C9orf72_RNA_6xSrG | /SPhos/rArArA rArArA rArGrG rGrGrC rCrGrG rGrGrC rCrGrG* rC* rG* rG* rG* rG* /3InvdT/ |
| G4_C9orf72_DNA_6xSG | /SPhos/rArArA rArArA rAGG GGC CGG GGC CGG* C*G*G* G*G* /3InvdT/ |
| G4_telo_DNA_6xSG | /SPhos/rArArA rArArA TAG GGT TAG GGT TAG GGT* T*A*G* G*G* /3InvdT/ |
| 26rA_G4_C9orf72_RNA_6xSrG | /SPhos/rArArA rArArA rArArA rArArA rArArA rArArA rArArG rGrGrG rCrCrG rGrGrG rCrCrG rGrGrG rC* rC* rG* rG* rG* rG* /3InvdT/ |
| 26rA_G4_C9orf72_DNA_6xSG | /SPhos/rArArA rArArA rArArA rArArA rArArA rArArA rArAG GGG CCG GGG CCG CCG GGG C*G*G* G*G* /3InvdT/ |
| 26rA_G4_telo_DNA_6xSG | /SPhos/rArArA rArArA rArArA rArArA rArArA rArArA rArArA rArAT AGG GTT AGG GTT AGG GT*T* A*G*G* G* /3InvdT/ |

^aSequences are listed in IDT format: RNA bases, r_—; RNA phosphorothioate bases, r_{—*}; DNA phosphorothioate bases, —*; 5' phosphate modification, /SPhos/; 2'-3'-dideoxycytidine [ddC] modification, /3ddC/; inverted-2'-deoxythymidine [InvdT] modification, /3InvdT/.

RESULTS AND DISCUSSION

Highly Efficient Synthesis of mocRNA by Ligation. To enable the conjugation between *in vitro* transcribed (IVT) mRNA and a synthetic oligo, each oligo was designed with the following elements (Figure 1a, Table 1): (1) a 5' phosphate and at least six unstructured RNA nucleotides at the 5' end of the oligos to ligate with the 3' terminus of IVT mRNAs by T4 RNA Ligase I; (2) a 3' blocking group (2'-3'-dideoxycytidine [ddC] or inverted-2'-deoxythymidine [InvdT]) to prevent oligo self-ligation; and (3) comparable lengths of poly(A) regions to enable reliable comparison of translation enhancement. The 3' blocking group of the oligo enables a large molar excess of oligo in the reaction to ensure nearly 100% conversion of the IVT mRNA to a mocRNA product (Figure 1a,b, Table 1).

To demonstrate the mocRNA expression system, we cloned a plasmid template containing a humanized Monster Green Fluorescent Protein (GFP) followed by a template-encoded poly(A) tail (plasmid: pCS2_GFP-60A), which ensures translatable mRNAs with homogeneous poly(A) lengths. The GFP-encoding mRNAs (GFP-60A) were synthesized using IVT by SP6 polymerase, with a 5' antireverse cap analog (ARCA) and 100% replacement of uridine with N¹-methylpseudouridine. The IVT mRNAs were further modified into mocRNAs by 3' oligo ligation using T4 RNA ligase I. The conjugation efficiency was determined via sequence-specific RNA cleavage, using RNase H and a DNA oligo targeting the 3' untranslated region (UTR), followed by gel electrophoresis to resolve conjugated and unconjugated mRNA 3' ends. The RNase H assay showed nearly 100% conjugation efficiency for all of the mocRNA constructs using the aforementioned GFP-60A mRNA (Figure 1b, Supporting Information Figure 1a), suggesting the general applicability of our conjugation strategy.

Nuclease-Resistant mocRNA Increases Protein Production and RNA Stability in Human Cells. Given that endogenous deadenylation machinery is a 3'-to-5' exonuclease complex and deadenylation is the rate-limiting step of canonical RNA decay inside cells, we reasoned that introducing nuclease-resistant elements at the 3' terminus after the poly(A) tail would be an effective way to increase

RNA translation capacity by keeping the poly(A) tail intact. To this end, we synthesized mocRNA constructs using synthetic oligos (3xSrA_ddC, 3xSrA_InvdT, 3xSrG_InvdT, and 6xSr(AG), Table 1) containing 3' terminal deadenylase-resistant modifications, such as phosphorothioate (PS) linkages¹⁸ and A-to-G substitutions.²² GFP-encoding mocRNA constructs were transfected into HeLa cells along with *E. coli* poly(A) polymerase (E-PAP) poly(A) tailed mCherry mRNA, which served as an internal transfection control. GFP/mCherry fluorescence intensity ratios were quantified at 24, 48, and 72 h time points after transfection with confocal microscopy. Fluorescence quantification showed that the control mocRNA construct, which contained an additional 29 nt-long poly(A) tract followed by a 3' ddC (29rA_ddC), increased GFP fluorescence by up to 69% in comparison with a mock ligation control (GFP-60A mRNA treated with ligase but no modified oligo). This increase was likely due to the extension of the poly(A) tail and possibly the presence of the chain-terminating nucleotide. Among all of the oligos containing terminal PS linkages, the unstructured single-stranded (ss) RNA oligo with six sequential phosphorothioates (6xSr(AG), sequence in Table 1) consistently provided the highest expression of GFP (290%–377% at 24–72 h, normalized to “mock ligation”) compared to the other modified oligos tested (Figure 2a,b; Supporting Information Table 2).

Given the success of PS-modified mRNAs, we hypothesized that 3' terminal RNase-resistant DNA linkages could similarly increase protein translation. However, the results demonstrated that the oligo containing 23 deoxyadenosines (23xdA_ddC) did not substantially enhance protein translation. In contrast, the telomere-derived DNA quadruplex (G4_telo_DNA_WT) sequence significantly enhanced protein translation (150%–170% at 24–72 h) compared to the unstructured “G to C” DNA oligo control ligation (Figure 2a,b; Supporting Information Table 2). These results suggest that mRNAs containing unstructured ssDNA at their 3' ends may remain susceptible to cellular nucleases, such as ssDNA-specific nucleases^{23,24} and CCR4 (a component of the deadenylation complex), which contains some ssDNase activity.²⁵ An alternative possibility is that unstructured

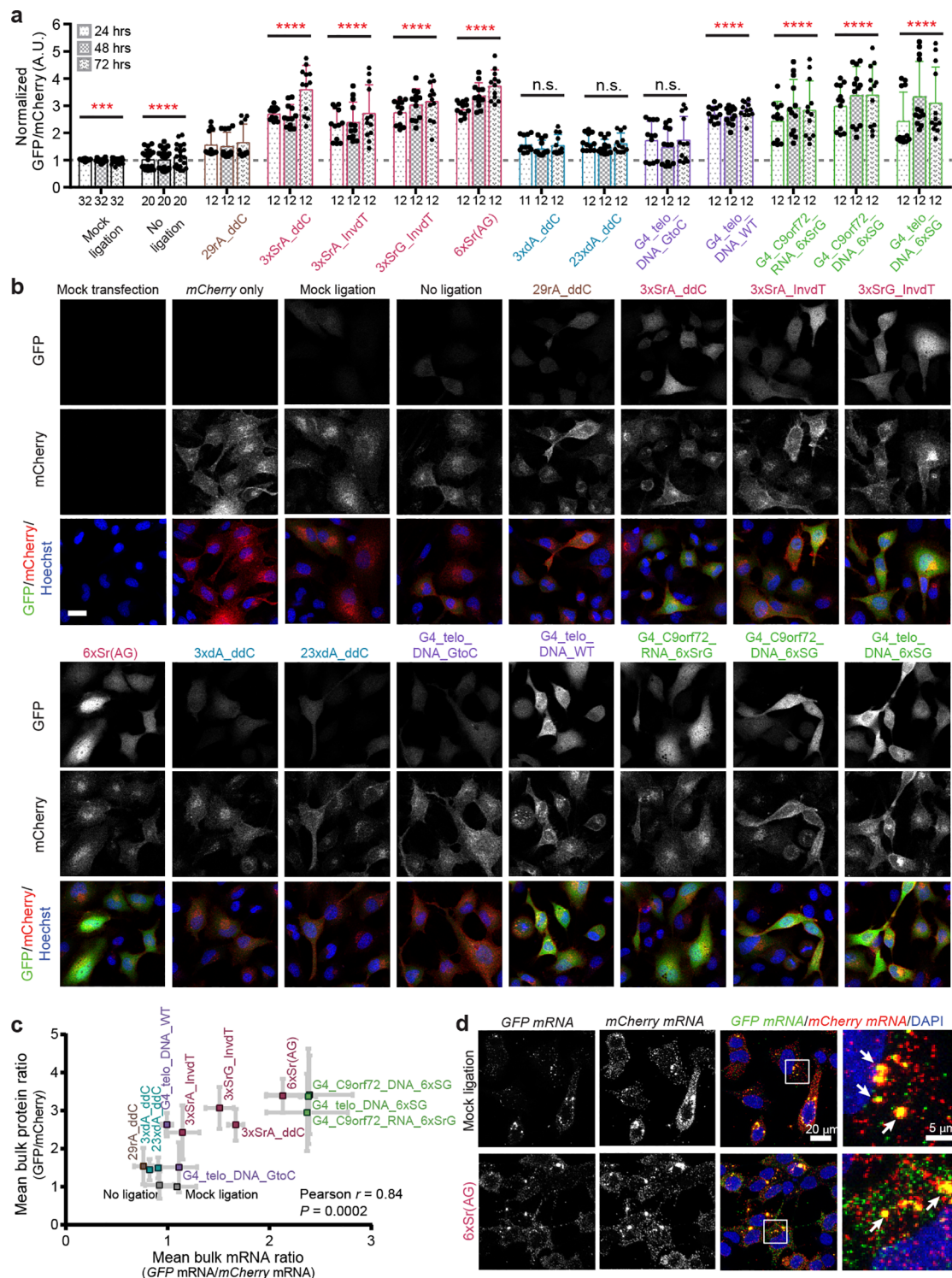


Figure 2. Enhanced protein production and RNA stability from mocRNAs in HeLa cells. (a) Barplots of GFP fluorescence signal normalized to mCherry fluorescence signal and the mock ligation control at 24, 48, and 72 h post-transfection. Gray dashed lines, $y = 1$; mean \pm s.d.; n fields of view (FOV) indicated under respective bars. Each condition had at least three biological replicates, of which four FOVs were imaged from each. P values were calculated by ordinary two-way ANOVA (Dunnett's multiple comparisons test, comparison of means across time points), with multiple comparisons to the sample 29rA_ddC. *** $P < 0.001$, **** $P < 0.0001$, n.s. $P > 0.05$. (b) Representative separate and overlay images of mCherry fluorescence (red), GFP fluorescence (green), and Hoechst nuclei staining (blue) in HeLa cells 48 h after transfection of the indicated RNA construct under the same confocal imaging setting. Scale bar, 25 μm . (c) Correlation of the means of bulk GFP/mCherry RNA ratios (RT-qPCR, mean \pm SEM, also see Supporting Information Table 3) and bulk GFP/mCherry fluorescence ratios (mean \pm s.d.) 48 h after transfection. (d) Representative images of STARmap amplicons representing GFP RNA (green) and mCherry RNA (red) *in situ* in HeLa cells fixed 48 h after transfection with indicated mRNA vectors, acquired under the same confocal imaging setting. DAPI (blue), nuclei. Colocalized GFP and mCherry amplicons (yellow) were potentially lipid transfection vesicles (white arrows) and thus excluded from downstream STARmap quantification of RNA species.

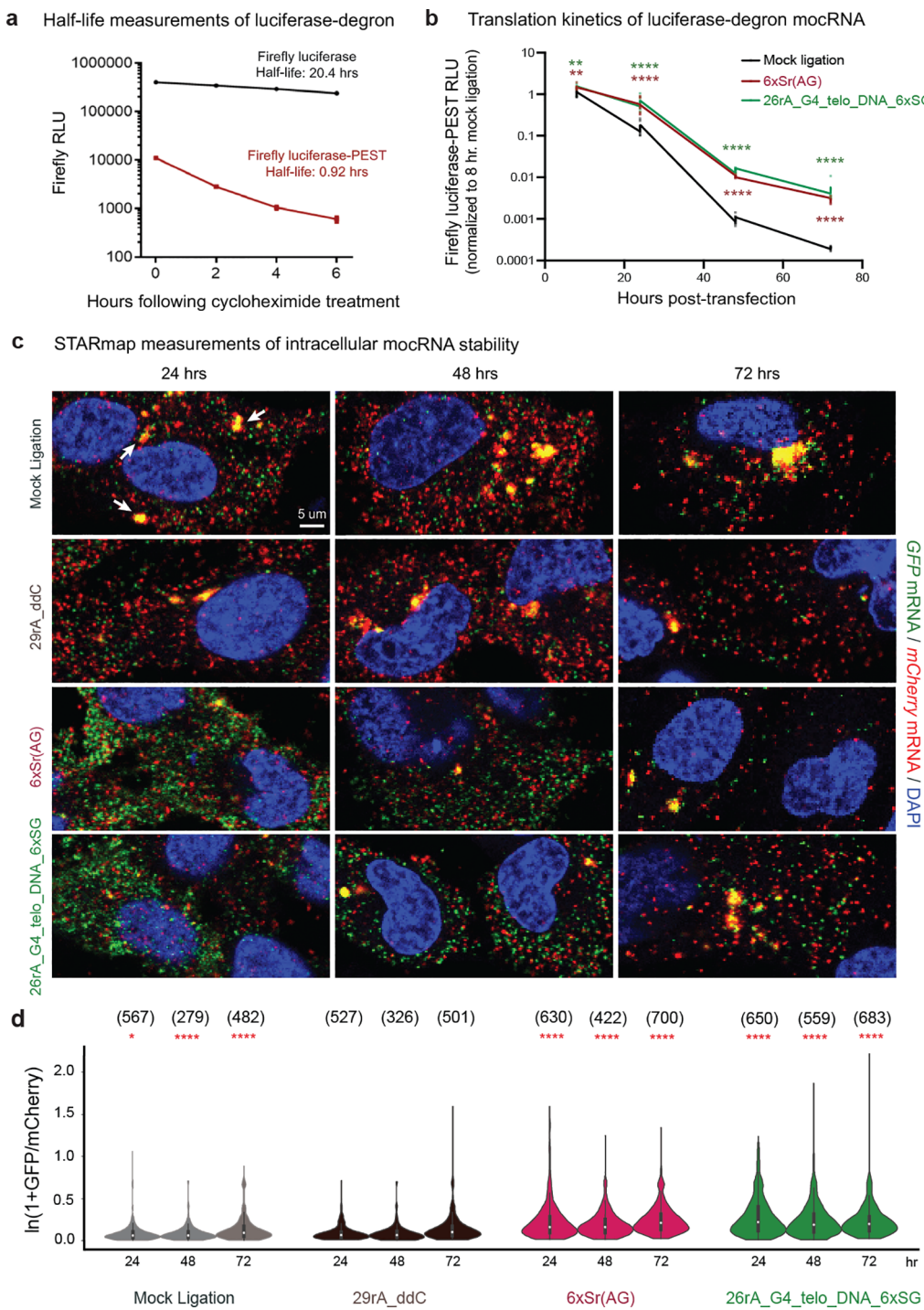


Figure 3. Kinetic characterization of optimized mocRNA constructs. (a) Kinetic characterization of Firefly luciferase-degron compared to an untagged luciferase. mRNAs encoding each protein were transfected into HeLa cells, which were treated with cycloheximide (CHX) at time = 0. Resulting RLU was measured in cells at 2-h intervals following CHX treatment, to estimate a decay half-life for proteins. (b) Firefly luciferase-degron RLU normalized to mock ligation signal (8 h post-transfection). Corresponding normalized Firefly RLU values at each time point were tested for significance using an ordinary one-way ANOVA test, compared to mock ligation for each time point. * $P < 0.05$, ** $P < 0.01$, *** $P < 0.001$, **** $P < 0.0001$. (c) Representative STARmap images (channel overlay) taken at 24, 48, and 72 h time points from mocRNA-transfected HeLa cells. Images were taken as single slices from Z-stacks obtained from each field of view. White arrows in mock ligation, 24 h sample, show representative transfection vesicles (regions of large size and overlapping GFP/mCherry signal). Green amplicons indicate GFP mRNA. Red amplicons indicate mCherry mRNA, and blue signals correspond to DAPI nuclear stain. Image contrast was adjusted equally among images in ImageJ. (d) Time course STARmap mRNA counts, quantification in mocRNA-transfected HeLa cells. GFP and mCherry mRNA species are counted, with the exclusion of large aggregates (i.e., transfection vesicles). Three biological replicates for each experimental condition, with four FOVs taken from each sample. Violin plot elements: lines, lower/upper adjacent values; bars, interquartile ranges; white dot, median. Single cell numbers are listed above corresponding distributions. Statistical testing is performed using Welch's *t* test with comparisons to 29rA_ddC at each respective time point. * $P < 0.05$, ** $P < 0.01$, *** $P < 0.001$, **** $P < 0.0001$.

ssDNA may trigger mRNA degradation *via* RNase H if they contain partial complementarity to mRNA sequences.²⁶ Collectively, the results indicate that mocRNAs containing a structured DNA quadruplex at the 3' terminus increase protein expression, while an unstructured ssDNA tail does not.

We further explored whether combining PS modifications with G4 secondary structures (PS+G4) could synergistically stabilize mocRNAs. The ssDNA and ssRNA G4 oligos containing six sequential PS linkages (G4_C9orf72_RNA_6xSrG, G4_C9orf72_DNA_6xSG, and G4_telo_DNA_6xSG) resulted in levels of enhanced translation similar to the mocRNAs containing an unstructured 6xSr(AG) oligo (Figure 2a,b; Supporting Information Table 2).

The enhanced translation of mocRNAs may have been due to either a reduced RNA degradation rate or a direct increase in the translational efficiency per mRNA, without affecting mRNA degradation kinetics. To verify the mechanism of translational enhancement, we performed RT-qPCR quantification on HeLa cells transfected with various mocRNA ligation constructs at 48 h post-transfection (Supporting Information Table 3). We found that the relative GFP/mCherry RNA ratios correlated well with the observed bulk GFP/mCherry protein fluorescence ratio for each construct (Figure 2c, Pearson $r = 0.84$, $P = 2e-4$; Supporting Information Figure 2b,c), suggesting that modified oligos enhance protein translation primarily by stabilizing mRNA quantities in cells.

Given the stochastic nature of lipid-mediated transfection and endosomal rupture, there can be a large variance in the number of transfected mRNAs across individual cells.²⁷ To characterize whether the observed translational enhancement of mocRNAs represented a general increase in translation throughout the entire cell population or if it resulted from a small set of high-expressing cells, we quantified the ratios of GFP/mCherry protein fluorescence and RNA copy numbers at the single-cell level. Single-cell fluorescence analyses of GFP/mCherry fluorescence ratios (Supporting Information Figure 2a) recapitulated the trends observed in bulk measurements (Figure 2a). We further quantified mRNA abundance in transfected cells using STARmap,²⁸ an *in situ* transcriptomic method capable of identifying target mRNA copy numbers in fixed cell or tissue samples at subcellular resolution (Figure 2d, Supporting Information Figure 2b). In the STARmap images, the green and red fluorescent puncta correspond to free "cytosolic" GFP-mocRNAs or mCherry mRNAs, respectively. Large "yellow" intracellular granules (due to overlapping red and green fluorescence) likely correspond to lipid transfection vesicles containing many copies of GFP-mocRNAs and mCherry mRNAs (Figure 2d). While RT-qPCR provides bulk measurements of mRNA (cytosolic and contained in the transfection reagent), STARmap enables the spatial separation of these two signals, enabling direct quantification of individual cytosolic mRNAs by filtering out signals from large aggregates. Importantly, the quantification of the cytosolic RNA fraction at the single-cell level indicates that the stabilization effects of mocRNAs also occur throughout the entire cell population (Supporting Information Figure 2c,d).

Protein and RNA Kinetics Show Increased Stability of mocRNAs in Cells. We reasoned that translation observed from the initial screen of PS+G4 oligos could be potentially confounded by the extension of the poly(A) tail by different lengths (26 rA's in 6xSr(AG) and 6 rA's in G4_C9orf72_RNA_6xSrG, G4_C9orf72_DNA_6xSG, and G4_telo_DNA_6xSG). To address this point directly, we performed a

comparison between 6xSr(AG) and redesigned longer PS+G4 oligos containing a similar number of rA's: 26rA_G4_C9orf72_RNA_6xSrG, 26rA_G4_C9orf72_DNA_6xSG, and 26rA_G4_telo_DNA_6xSG. The HeLa expression time course indicated that 6xSr(AG) outperformed the 26rA-containing C9orf72 oligos in expression enhancement. However, 26rA_G4_telo_DNA_6xSG demonstrated modest translation enhancements over 6xSr(AG) (17–24% between 24 and 72 h, Supporting Information Figure 3a). These data suggest that specific telomere structures may add relatively low levels of additional stabilization, beyond the stabilization afforded by PS linkages. Due to the similar levels of expression between 6xSr(AG) and 26rA_G4_telo_DNA_6xSG mocRNAs, we proceeded with using these two oligos for downstream kinetic analysis of protein expression.

To characterize the kinetics of mocRNA translation at varying time points, we generated mocRNAs encoding a degron-tagged Firefly luciferase. The degron (PEST derived from mouse ornithine decarboxylase²⁹) reduced luciferase half-life in HeLa cells from 20.4 h to an estimated 0.92 h (Figure 3a). We generated luciferase-PEST mocRNAs containing our two best-performing oligos: 6xSr(AG) and 26rA_G4_telo_DNA_6xSG, and we recorded luminescence as a function of time following mRNA transfection into HeLa cells. At 8 h post-transfection, 6xSr(AG) and 26rA_G4_telo_DNA_6xSG mocRNAs (encoding luciferase-degron) demonstrated slightly greater levels of translation than the mock ligation (44% and 39% greater signal, respectively). However, by 48 and 72 h, both mocRNAs substantially outperformed the mock ligation, with 6xSr(AG) demonstrating 10-fold and 15-fold more signal, respectively, and 26rA_G4_telo_DNA_6xSG demonstrating 15-fold and 25-fold more signal (Figure 3b). This translational enhancement was not due to differences in transfection efficiency between samples, as comparable significant differences were not observed in the translation of a cotransfected Renilla luciferase mRNA internal control (Supporting Information Figure 3c). The observed kinetics of mocRNA translation are consistent with 6xSr(AG) and 26rA_G4_telo_DNA_6xSG possessing intact poly(A) tails at these time points (enabling translation), in contrast to the mock ligation. Furthermore, *in vitro* translation experiments performed on mocRNAs did not show substantial differences in translation efficiency between mocRNA and controls (Supporting Information Figure 3b). This indicates that increased protein expression from mocRNA is primarily attributed to enhanced mRNA lifetime, rather than enhanced translation initiation efficiency.

We further verified the kinetics of mocRNA decay in cells by performing *in situ* mRNA visualization using STARmap at 24, 48, and 72 h post-transfection into HeLa cells (Figure 3c). We transfected GFP-60A mocRNAs containing 29rA_ddC, 6xSr(AG), or 26rA_G4_telo_DNA_6xSG into HeLa cells and quantified relative mRNA abundance over time. The 6xSr(AG) mocRNA samples displayed 1.7–2.5-fold higher GFP/mCherry mRNA count ratios (averaged from single cells) than 29rA_ddC at each time point. Additionally, 26rA_G4_telo_DNA_6xSG had 1.7–3.1-fold higher GFP/mCherry mRNA count ratios compared to the 29rA_ddC control at each time point (Figure 3d).

mocRNA Outperforms Alternative Strategies for mRNA Modification. Previous work has reported that PS linkages incorporated by *E. coli* poly(A) polymerase (E-PAP) into the poly(A) tail can enhance mRNA stability.¹⁸ Here, we

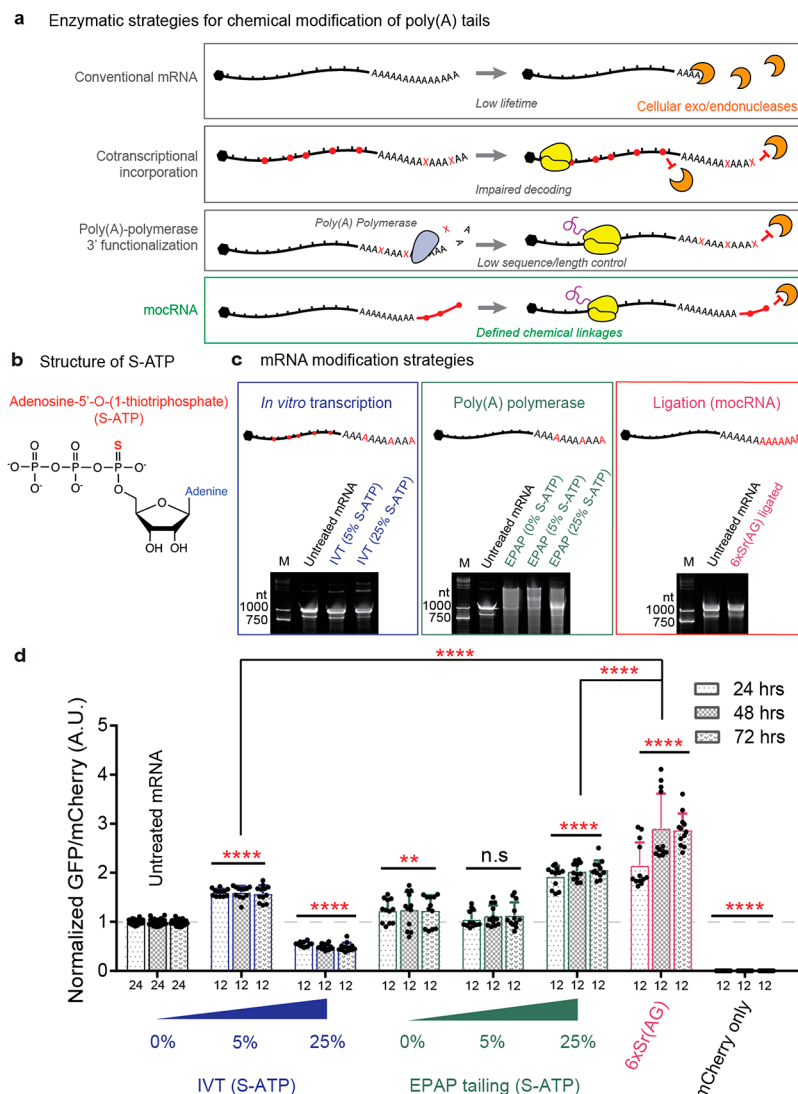


Figure 4. Performance comparison of different mRNA modification strategies. (a) Schematics of general chemical strategies to increase mRNA exo- and endonuclease resistance through the incorporation of modified nucleotide triphosphates (NTPs). Strategies boxed in gray are previously reported methods, and the ligation strategy (green) is explored thoroughly in this study. X, modified nucleoside. (b) Chemical structure of adenosine-5'-O-(1-thiotriphosphate) (S-ATP) used in E-PAP and IVT spike-in reactions. Sulfur modification of alpha phosphate, when incorporated into RNA, is identical to a phosphorothioate (PS) linkage (shown in Figure 1b). (c) Schematics depicting the different strategies of incorporation of phosphorothioate (PS) linkages into mRNA. RNA polymerase (i.e., cotranscriptional) and poly(A) polymerase incorporation of adenosine-5'-O-(1-thiotriphosphate) (S-ATP) were used to install nuclease-resistant PS linkages into mRNA. Insets: denaturing gel showing the effects of each modification strategy on the length distribution of mRNAs. Red A's, chemically modified adenosines; black A's, unmodified adenosines. M, Marker; Century-Plus RNA Markers. (d) Barplots of GFP protein abundance from modified GFP mRNA generated various strategies, normalized to mCherry and the average of the untreated mRNA control at each time point (24, 48, and 72 h) after transfection into HeLa cells. Mean \pm s.d.; n, number of FOVs indicated under respective bars. Each condition consisted of at least three biological replicates, of which four FOVs were imaged from each. Red line: $y = 1$. P values are calculated by ordinary two-way ANOVA (Dunnett's multiple comparisons test, comparison of means across time points), with multiple comparisons to untreated mRNA unless specified in the figure. ** $P < 0.01$, **** $P < 0.0001$, n.s. $P > 0.05$.

also explored the E-PAP modification strategy of poly(A) tails. We screened a panel of chemically modified ATP derivatives (XATP) by introducing XATP spike-ins into poly(A) tailing reactions on a capped GFP mRNA containing N¹-methyl-pseudouridine instead of uridine (Supporting Information Figure 4). We cotransfected HeLa cells with various tail-modified GFP mRNAs along with an internal transfection control, tail-unmodified mCherry mRNAs (100% ATP, E-PAP tailed), and monitored the GFP/mCherry fluorescence ratio over a three-day time course. The initial screen in HeLa cell experiments revealed that poly(A) modification by XATP

spike-ins increased normalized GFP production in comparison with the unmodified poly(A) construct, particularly for dATP (2'-deoxyadenosine triphosphate, 25–62% increase in normalized GFP/mCherry) and S-ATP (adenosine-5'-O-(1-thiotriphosphate), 42–91% increase; Supporting Information Figure 4). S-ATP spike-in resulted in the greatest enhancement of GFP expression (consistent with previously reported work¹⁸) and thus was used to compare different mRNA modification strategies (Figure 4a).

We compared 6xSr(AG) to GFP-60A mRNAs functionalized by S-ATP, via IVT or E-PAP incorporation (Figure 4a–

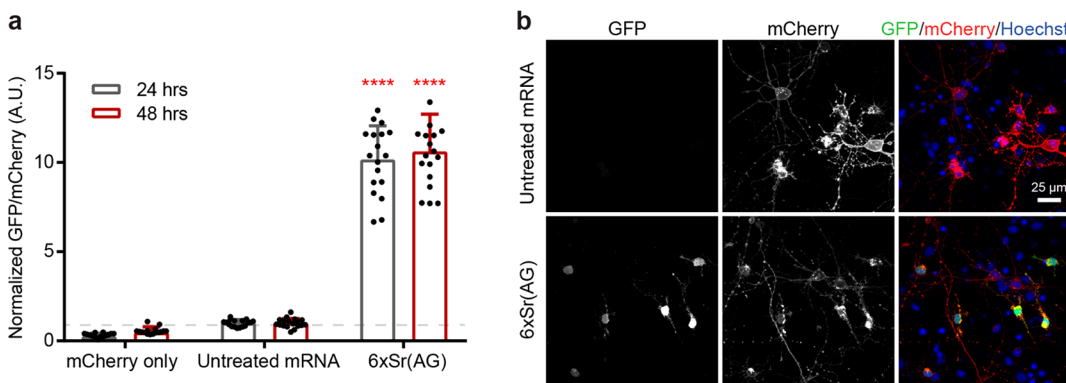


Figure 5. 6xSr(AG) mocRNA boosts protein production in primary neuronal cultures. (a) Bar plots of GFP protein abundance normalized to mCherry and the “untreated” control in neurons 24 and 48 h after transfection. Mean \pm s.d., n (FOV) = 18. Each condition consisted of at least three biological replicates, of which six FOV/stacks were imaged from each. Gray dashed line: $y = 1$. P values were calculated with ordinary two-way ANOVA (Dunnett’s multiple comparisons test) compared to the untreated sample for each separate time point. *** $P < 0.0001$. (b) Representative images of GFP and mCherry fluorescence in neurons 24 h after transfection imaged under the same confocal microscopy setting. Hoechst (blue), nuclei. Scale bar, 25 μ m.

c) in RNA length homogeneity and protein production. mocRNAs and IVT-modified constructs showed uniform length distributions, whereas E-PAP-tailed mRNAs have a wide distribution of tailing lengths, with shorter lengths as the percentage of S-ATP spike-in increased (Figure 4c). Using mCherry mRNA (E-PAP tailed with 100% rA) as an internal transfection control, we quantified the GFP/mCherry fluorescence ratios at 24, 48, and 72 h post-transfection in HeLa cells. After normalizing to the untreated GFP-60A control, the 6xSr(AG) mocRNA resulted in the highest enhancement of GFP expression at various times post-transfection (24 h, 214 \pm 45%; 48 h, 289 \pm 68%; 72 h, 286 \pm 32%; mean \pm s.d.; Figure 4d). Among all of the E-PAP tailed mRNA constructs, 25% S-ATP spike-in had the highest enhancement of GFP expression in comparison with the untreated GFP-60A control (24 h, 93 \pm 21% increase). IVT-mediated incorporation of S-ATP proved beneficial for small percentages of modified ATP (24 h, 5% S-ATP: 160 \pm 7%); we observed decreased translation of the reporter at 25% S-ATP (54 \pm 5%) compared to the untreated GFP-60A mRNA. Overall, this systematic comparison between different modification methods of mRNA tails demonstrated the superior performance of mocRNAs over E-PAP and IVT-modified mRNA (Figure 4d).

mocRNA Constructs Enhance Protein Expression in Primary Rat Cortical Neuronal Cultures. Neurons are the main therapeutic targets in a variety of brain and nervous system-related diseases.^{30,31} While chemical/lipid-mediated transfection of DNA plasmids demonstrates limited expression efficiency in postmitotic cells, such as neurons, mRNA transfection is an alternative to introduce transgenic protein expression in neurons with potentially higher efficiency.³² To explore whether mocRNA could increase protein production in primary cell culture, we tested the modified constructs in primary cultures of rat cortical neurons.

GFP mocRNA prepared by 6xSr(AG) oligos and unligated controls were cotransfected with mCherry mRNA (E-PAP tailed with 100% rA, transfection control) for comparisons at 24 and 48 h post-transfection (Figure 5a). In comparison with unligated GFP samples, the GFP expression of 6xSr(AG) mocRNA samples showed an order of magnitude higher expression at both time points (24 h, 1015 \pm 190%; 48 h, 1061 \pm 210; Figure 5a,b, Supporting Information Table 4). These results demonstrated that mocRNAs can offer robust enhance-

ment of protein expression in neuronal cell culture, compared to conventional mRNA vectors (Figure 5).

mocRNA Retains Similar Toxicity Profiles to Therapeutic mRNA. Unmodified IVT mRNA triggers strong immune responses upon transfection, which suppress its protein production.^{10–12} While 100% replacement of uridine with N¹-methylpsudouridine is used in therapeutic mRNA (and mocRNA) preparations to minimize immune toxicity,¹² we further evaluated if chain-terminating nucleotides, PS linkages, or the covalent DNA–RNA bonds introduced by the synthetic oligos into mocRNAs would trigger additional cellular toxicity. First, we quantified cell numbers from imaging data displayed in Figure 2, to check for substantial decreases in cell proliferation and viability. We did not observe significant decreases in HeLa cell numbers between any mocRNA condition and the unligated mRNA control (Supporting Information Figure 5a). Additionally, we checked for innate immune stimulation in HeLa cells through RT-qPCR measurements of *IFNB1* mRNA on the 48-h post-transfection samples shown in Figure 2. *IFNB1* upregulation is a consequence of RIG-I and MDAS activation, which are innate immune sensors that recognize foreign RNA species.^{33–35} Positive controls of unmodified GFP mRNA (100% uridine) and poly(I:C) transfection (a potent RIG-I agonist³⁶) induced statistically significant *IFNB1* mRNA upregulation when compared to the 29rA_ddC mocRNA control (Welch’s *t*-test). However, no significant differences were observed between any mocRNAs, unligated mRNA, and the transfection only control (Supporting Information Figure 5b). These results indicate that mocRNAs do not inherently increase innate immune responses beyond untreated mRNAs, at least for the constructs explored in this study.

Finally, we analyzed mocRNA-mediated toxicity in neurons, using live–dead cell staining on transfected rat cortical neuron cultures (with Hoechst stain and NucRed Dead 647). We calculated the percentage of dead neurons in each culture condition, to test for differences in cellular toxicity between mocRNA and conventional mRNA transfection. We did not observe significant differences in neuronal toxicity caused by 6xSr(AG) ligation, compared to a transfection control (Supporting Information Figure 5c). Taken together, these results suggest that the modifications identified in this study

did not substantially alter the toxicity profiles of mRNAs in the cell cultures tested.

SUMMARY AND CONCLUSIONS

Existing methods that utilize poly(A) polymerase to synthesize chemically modified poly(A) tails often result in wide distributions of tail lengths that could complicate batch-to-batch homogeneity and cannot precisely control modification sites. In contrast, mocRNA synthesis demonstrates nearly 100% yields and can fully preserve mRNA homogeneity, which makes it compatible with existing pipelines for the development of mRNA therapeutics. More importantly, the mocRNA expression system can introduce chemical modifications that cannot be incorporated by RNA polymerases and enables precise control of modification sites to maximize the effects of RNA modifications. As the first demonstration, mocRNA with clustered nuclease-resistant motifs at the 3' terminus enhanced protein expression by protecting the poly(A) tail of mRNA vectors. Fluorescent protein measurements demonstrated that mocRNAs containing 3' terminal PS linkages increased protein production by factors of 2–4 in human HeLa cell lines (Figure 2a) and by 10-fold in primary rat cortical neuronal cultures (Figure 5a). Combined bulk RT-qPCR measurement and single-cell resolved *in situ* STARmap measurements indicate that mocRNAs containing 3' terminal PS modifications and specific telomere sequences improve protein expression primarily by stabilizing RNAs (Figure 2c–d, Figure 3c–d, Supporting Information Figure 3a).³⁷ Those mocRNA constructs have higher translation capacity than existing variants of mRNA vectors relying on random incorporation of modified NTPs during IVT and polyadenylation^{14,15,18} (Figure 4d).

In summary, we developed a modular, programmable, and effective strategy to synthesize mocRNAs, enabling diversified and precise chemical modifications of RNA vectors to enhance protein translation capacity and RNA stability. mocRNAs can potentially be combined with other types of modification strategies, such as poly(A) binding protein (PABP)-binding oligos,³⁸ hydrolysis-resistant 7-methylguanosine caps,^{39,40} modified 5' UTR regions,⁴¹ and other types of modified nucleotides in the mRNA body.⁴² We believe that the mocRNA design could serve as a generalizable platform for integrating organic synthesis with enzymatic synthesis, to diversify chemical moieties and boost functional efficacy of RNA-based protein expression systems.

METHODS

Plasmid Cloning, Characterization, and Purification. We obtained hMGFP and mCherry-encoding plasmids (pCS2_hMGFP and pCS2_mCherry, respectively) from Xiao Wang. These plasmids contained (in order) an SP6 promoter sequence, a 5' UTR, a fluorescent protein coding sequence (CDS), 3' UTR, and NotI restriction cut site. Sequences can be found in the original reference.⁴³

We used the Q5 Site-Directed Mutagenesis Kit (NEB: E0554S) to perform PCRs on template plasmids using primers (Supporting Information Table 1) containing site-specific modifications. This was followed by KLD enzyme treatment, then transformation into NEB StabI cells (NEB: C3040H) for isolation using the ZymoPURE plasmid miniprep kit (Zymo: D4209) and Sanger sequencing through Genewiz.

For the site-specific installation of 60xA template-encoded poly(A) tails in front of an Esp3I site, two sequential rounds of cloning were performed using Q5 site-directed mutagenesis. The first round of cloning installed an Esp3I restriction site 5' of the previous NotI

restriction site (Esp3I_insert_F and Esp3I_insert_R). The resulting Sanger sequencing-verified plasmid was used as a template for the installation of the 60xA poly(A) tail (60A_insert_F and 60A_insert_R). The clone selected from the second round of cloning was verified using Sanger sequencing. See Supporting Information Table 1 for primer sequences. The name of the construct containing ~60-nt-long template-encoded tails prior to the Esp3I site was pCS2_hMGFP-60A.

Firefly luciferase constructs were generated first by deletion of the hMGFP coding region from the pCS2_hMGFP-60A vector using PCR. Next, the Firefly luciferase coding sequence was PCR-amplified from pmirGLO Dual-Luciferase miRNA Target Expression Vector (Promega: E1330), with PCR primers designed to contain 15–25 nucleotide complementary overhang regions to the vector of interest. The vector and insert were assembled using NEBuilder HiFi DNA Assembly Master Mix (NEB: E2621S), transformed into StabI cells, and sequence-verified by Sanger sequencing. Renilla luciferase constructs were cloned by an analogous process to Firefly luciferase, except with a Renilla luciferase coding sequence from the pmirGLO vector.

The destabilized Firefly luciferase construct (i.e., Firefly-PEST) contains a degron derived from mouse ornithine decarboxylase.²⁹ The aforementioned Firefly luciferase vector was PCR-linearized around the stop codon, into which a GeneBlock (IDT, human codon-optimized) encoding the PEST sequence was inserted using the NEBuilder HiFi method.

mRNA Synthesis and Characterization. GFP mRNA was synthesized from the pCS2_hMGFP-60A plasmid, which contained an SP6 promoter, followed by hMGFP CDS and template-encoded poly(A) tail. Plasmids were linearized by a single Esp3I (NEB: R0734S) site located immediately 3' of the poly(A) region, which was installed during cloning. Linearized plasmids were then purified using the DNA Clean & Concentrator-25 kit from Zymo Research (D4033) and checked for purity via agarose gel electrophoresis. Capped, modified mRNA was prepared using the SP6 enzyme and reaction buffer from the mMESSAGE mMACHINE SP6 Transcription Kit (ThermoFisher Scientific: AM1340). We replaced the 2× NTP/Cap solution provided by the kit with a 2× NTP/Cap preparation of our own, containing 10 mM ATP (NEB: N0451AVIAL), 10 mM CTP (NEB: N0454AVIAL), 2 mM GTP (NEB: N0452AVIAL), 8 mM 3'-O-Me-m7G(5')ppp(5')G RNA cap structure analog (NEB: S1411S), and 10 mM N¹-methylpsudouridine-5'-triphosphate (TriLink Biotechnologies: N-1081-1). We added SUPERase-In RNase Inhibitor (ThermoFisher Scientific: AM2694) to a final concentration of 1:20 (v/v). Following IVT reaction assembly and incubation at 37 °C for 2–4 h, reactions were treated with 1–2 μL of TURBO DNase (provided in AM1340) for 1 h at 37 °C prior to reaction purification using MEGAclear Transcription Clean-Up Kit (ThermoFisher Scientific: AM1908). We added Superase-In RNase Inhibitor to purified mRNA samples to a final concentration of 1:50 (v/v) and stored samples at –80 °C for long-term storage. Purified mRNA was nanodropped to estimate concentration prior to ligations, and mRNAs and mocRNAs were measured using the Qubit RNA HS Assay (ThermoFisher Scientific: Q32852) for normalization immediately prior to transfection for cell-based testing.

For the preparation of poly(A) polymerase-tailed mRNA (Supporting Information Figure 4), we used dsDNA templates generated by linearization of pCS2_hMGFP and pCS2_mCherry plasmids using NotI-HF (NEB: R3189S) and column purified digested products using Zymo DNA Clean & Concentrator-25. We performed *in vitro* transcription using the protocol described above, except after TURBO DNase digestion, we included the extra step of poly(A) tailing using the E-PAP Poly(A) Tailing Kit (ThermoFisher Scientific: AM1350). Purification and storage of mRNA were as described above (e.g., using MEGAclear transcription cleanup kit).

For Figure 4, adenosine-5'-O-(1-thiotriphosphate) spike-in mRNAs were synthesized using a modified protocol to the one listed above. We used adenosine-5'-O-(1-thiotriphosphate) (S-ATP) for cotranscriptional incorporation experiments. We observed qualitative differences in S-ATP incorporation when we used stock tubes that

had been opened previously, possibly due to oxidation. For this reason, we used brand new tubes prior to every tailing experiment, to limit the effects of possible oxidation as a confounding factor in our experiments. We performed S-ATP *in vitro* transcription reactions with the same setup as listed above, but we replaced our final 5 mM ATP in the reaction with either 4.75 mM ATP + 0.25 mM S-ATP (5% S-ATP incorporation) or 3.75 mM ATP + 1.25 mM S-ATP (25% S-ATP). We used IVT templates containing our GFP coding sequence with a 60xA template-encoded poly(A) tail.

Modified *E. coli* Poly(A) Polymerase Tailing. For modified E-PAP tailing experiments in Supporting Information Figure 4, our substrate was an untailed GFP mRNA generated from IVT's on a NotI-HF linearized pCS2_hMGFP template (see previous section for IVT protocol). Our protocol utilized the enzyme and buffer from the E-PAP Poly(A) Tailing Kit (ThermoFisher Scientific: AM1350). We prepared “10 mM total” ATP stock solutions for each modified ATP spike-in, such that a specific percentage of ATP was replaced by a modified ATP derivative (XATP). For example, 25% dATP samples would require the assembly of a 2.5 mM dATP, 7.5 mM ATP stock solution. Tailing reactions were assembled as follows: 1.5 μ g of untailed GFP mRNA; 5 μ L of 5X E-PAP buffer; 2.5 μ L of 10 mM XATP:ATP stock solution (different for each sample); 2.5 μ L of 25 mM MnCl₂; 1 μ L of Superase-In RNase Inhibitor; 1 μ L of E-PAP enzyme; and nuclease-free water up to a total volume of 25 μ L. Reactions were incubated at 37 °C for 1 h, then quenched with the addition of 0.5 μ L of 500 mM EDTA. These tailed mRNAs were then column purified using the Monarch RNA cleanup kit (50 μ g; NEB: T2040S). Superase-In RNase Inhibitor was added to purified mRNA to a final dilution of 1:50 (v/v), and mRNA was stored at -80 °C prior to transfection.

We used the following modified ATP derivatives (XATPs) in our experiments: adenosine 5'-triphosphate (ATP; NEB: P0756S); N⁶-methyladenosine-5'-triphosphate (TriLink Biotechnologies: N-1013-1); 2'-O-methyladenosine-5'-triphosphate (TriLink Biotechnologies: N-1015-1); adenosine-5'-O-(1-thiotriphosphate) (TriLink Biotechnologies: N-8005-1); dATP solution (NEB: N0440S); 2'-amino-2'-deoxyadenosine-5'-triphosphate (TriLink Biotechnologies: N-1046-1).

For modified E-PAP-tailing seen in Figure 4 (methods comparison), we performed E-PAP tailing using our hMGFP-encoding mRNA containing a template-encoded 60A tail (in contrast to Supporting Information Figure 4). We used adenosine-5'-O-(1-thiotriphosphate) (S-ATP) for cotranscriptional or modified poly(A) tailing experiments. We observed qualitative differences in S-ATP incorporation when we used stock tubes that had been opened previously, potentially due to oxidation. For this reason, we used brand new tubes prior to every tailing experiment, to limit the effects of possible oxidation as a confounding factor in our experiments. We otherwise set up E-PAP tailing reactions (with S-ATP spike-ins) consistently with the protocol described earlier.

Modified oligo 3' End Ligations. Ligation reactions were performed using T4 RNA Ligase I (Promega: M1051). Reactions were assembled as follows: 2 μ g of GFP mRNA; 200 pmol of the synthetic oligo; 2 μ L of Superase-In RNase Inhibitor; 20 μ L of 50% PEG-8000; 5 μ L of 100% DMSO; 5 μ L of 10X T4 RNA ligase buffer; 5–7.5 μ L of T4 RNA ligase (Promega); and nuclease-free water to a total reaction volume of 50 μ L. Reactions were incubated at 37 °C for 30 min, followed by inactivation of the reaction *via* the addition of 1 μ L of 500 mM EDTA at pH 8.0. Reactions were diluted by the addition of one volume of nuclease-free water (e.g., 50 μ L), followed by the addition of 0.5 volumes of AMPure XP (Beckman Coulter: A63880) containing 1 μ L of Superase-In (e.g., 25 μ L). Reactions were purified according to the manufacturer's protocol, and mRNA was eluted from AMPure beads using nuclease-free water containing Superase-In at a 1:50 (v/v) ratio. mRNA samples that appeared to contain residual oligo on a gel were purified a second time using AMPure XP beads.

For ligations that were incomplete according to our RNase H gel-based assay, we performed ligations using a modified condition, in which DMSO was omitted from the reaction. This generally resulted

in more efficient ligation, when necessary. For ligation-prepared samples shown in Figures 3, 4, and 5, we used the modified protocol for ligations, as this was generally more efficient. For Firefly luciferase and Firefly-PEST mRNA ligations, these were purified using 2 \times serial Ampure XP bead clean-ups, using a 1:1 bead volume to mRNA volume. For example, a 50 μ L ligation reaction was cleaned up using 50 μ L of Ampure XP beads (supplemented with 2 μ L Superase-In). Following elution of the product mRNA, a second cleanup was performed using an equal volume of beads to the eluted mRNA product.

RNase H Assays. We prepared a potassium chloride (KCl) stock solution used for annealing an ssDNA oligo to mRNA prior to RNase H assays. Our annealing stock solution contained 50 mM KCl, 2.5 mM EDTA, and 1:100 (v/v) Superase-In RNase inhibitor, brought to its final volume using nuclease free water. The ssDNA probe (RNaseH_probe_GFP) was ordered from IDT and sequence listed in Supporting Information Table 1.

The following reaction was prepared to anneal mRNA to the aforementioned ssDNA probe: 200 ng of purified mRNA sample (ligated or unligated), 2 pmol of RNaseH_probe_GFP, 2 μ L of annealing stock solution (50 mM KCl, 2.5 mM EDTA, 1:100 Superase-In), and nuclease-free water up to a total volume of 10 μ L. Reactions were denatured at 70 °C for 5 min, followed by cooling to RT at a rate of 0.2 °C/s in a benchtop thermocycler. Following probe annealing, 1 μ L of Thermostable RNase H (NEB: M0523S) and 1 μ L of the 10X buffer were added to each reaction, which was incubated at 50 °C for 30 min. Following reaction incubation, samples were digested by the addition of 1 μ L of Proteinase K (ThermoFisher Scientific: 25530049) and incubated at RT for 5 min. Subsequently, samples were mixed with one volume of Gel Loading Buffer II (ThermoFisher Scientific: AM8546G), which had been supplemented with EDTA to a final concentration of 50 mM. Samples in 1X loading buffer were denatured at 70 °C for 3–5 min prior to loading and resolution on 6% Novex TBE-Urea Gels (ThermoFisher Scientific: EC68655BOX), run in 1X Tris-borate-EDTA (TBE) buffer. The ladder used for gels was Century-Plus RNA Markers (ThermoFisher Scientific: AM7145). All gels were stained in 1X SYBR Gold (ThermoFisher Scientific: S11494) in 1X TBE buffer for 5–15 min prior to visualization using the BioRad ChemiDoc MP Imaging System (12003154) or the MP Imager (Universal Hood III), and images were exported using the corresponding Image Lab software.

Mammalian Cell Culture and mRNA Transfection. HeLa cells (CCL-2, ATCC) were maintained in DMEM culture media (ThermoFisher 11995) containing 10% FBS in a 37 °C incubator with 5% CO₂ and passaged at a ratio of 1:8 every 3 days. The cell culture is confirmed free of mycoplasma contamination regularly with Hoechst staining and microscopy imaging.

On the day before mRNA transfection, the cells were seeded at 75% confluence in individual wells on a 12-well plate. The day after, 500 ng of *mCherry* (internal control) mRNA and 500 ng of GFP mRNA with synthetic tails or other modifications (concentrations determined by Qubit) were transfected into each well using 3 μ L of Lipofectamine MessengerMAX Transfection Reagent (ThermoFisher, LMRNA003). Additional controls that contain only *mCherry* mRNA, or only transfection reagents, or nontransfected cells are included. After a 6-h incubation, the lipofectamine/mRNA transfection mixture was removed, and cells were rinsed once with 1xDPBS and trypsinized to reseed into three glass-bottom 24-well plates (MatTek, P24G-1.5–13-F, poly-D-lysine coated) at a ratio of 6:4:3, respectively, for fluorescent protein quantification at 24, 48, and 72 h after transfection.

Freshly dissociated rat primary cortical neurons were kindly provided by Sheng Lab at the Broad Institute. Briefly, rat cortical neuronal cultures were prepared from embryonic day 18 (E18) embryos from CO₂-euthanized pregnant Sprague–Dawley rats (Charles River Laboratories). Embryo cortices were dissected in ice-cold Hank's Balanced Salt Solution (HBSS, Gibco, 14175-095) supplemented with 100 U/mL of penicillin/streptomycin (Gibco, 15140-122). Cortical tissues were washed three times with 4 °C PBS (Sigma, D8537), digested in 0.25% Trypsin-EDTA (Gibco, 25200-

056) for 20 min at 37 °C, and then washed again three times with RT PBS. Cortical tissue was gently dissociated in 37 °C NBActiv4 media (Brainbits, NB4-500) and centrifuged at 300g for 5 min. The pellet was resuspended in fresh NBActiv4 and passed through a 70 µm filter (Corning, 352350).

Neurons were seeded at a density of $1 \times 10^5/\text{cm}^2$ on poly-D-lysine coated (Sigma, A-003-E, 50 µg/mL for at least one hour at RT followed by three rinses with sterile distilled H₂O and air-dry) 24-well glass-bottom plates (MatTek, P24G-1.5-13-F) in 0.5 mL of NbActiv4 media with half of the media changed every 4 days. On SDIV, neurons in 24-well plates were transfected with 250 ng of mCherry (internal control) mRNA and 250 ng of GFP mRNA with synthetic tails (concentrations determined by Qubit) mixed with 1.5 µL of Lipofectamine MessengerMAX Transfection Reagent (ThermoFisher, LMRNA003). The neurons were incubated with the transfection mixture for 2 h before changing back to the normal culture media (half old, half fresh). Procedures for rat neuronal culture were reviewed and approved for use by the Broad Institutional Animal Care and Use Committee. All procedures involving animals were in accordance with the US National Institutes of Health Guide for the Care and Use of Laboratory Animals.

Confocal Imaging and Quantification of Fluorescent Proteins. Before fluorescent protein imaging, the culture media were removed, and the cells were rinsed with 1xDPBS once before being incubated in the nuclei staining media (FluoroBrite DMEM [ThermoFisher, A1896701] with 1:2000 dilution of Hoechst 33342 [ThermoFisher, 62249]) at 37 °C for 10 min.

For HeLa cells, confocal images of the nuclei (Hoechst), GFP, and mCherry were taken by Leica Stellaris 8 with a 10× air objective at a pixel size of 900 × 900 nm. Four representative fields of view were taken for each well, one from each quadrant. For neurons, confocal image stacks of the nuclei (Hoechst), GFP, and mCherry are taken by Leica Stellaris 8 with a 25× water immersion objective at a pixel size of 450 × 450 nm and step size of 1 µm for nine steps. Six representative fields of view are taken for each well (Figure 5). For toxicity measurements in neurons, we added NucRed Dead 647 (Invitrogen: R37113) to the Fluorobrite staining media prior to imaging and used the corresponding channel to obtain images for the nuclei of dead cells. The same imaging setting was used for all the samples to be compared. Excitation/detection wavelengths are as follows: Hoechst, Diode 405 nm/~[430–480] nm; GFP, WLL 489 nm/~[500–576] nm; mCherry, WLL 587 nm/~[602–676] nm. CellProfiler 4.0.7⁴⁴ was used to calculate the number of objects in the Hoechst (e.g., total number of nuclei) versus NucRed Dead channel (e.g., dead nuclei), to yield fraction dead neurons in each field of view.

For bulk analyses in cultured neurons (Figure 2a), first, the mCherry intensity and GFP intensity in each image were measured. The average fluorescence signals in the mCherry channel and GFP channel in the “transfection only” samples were considered as background signals. Background signals were subtracted from each figure. Finally, the ratio between GFP intensity and mCherry intensity in each image was calculated. And outliers within each sample, determined by GraphPad Prism 9, were removed. The means of the ratios between GFP intensity and mCherry intensity in all the “untreated mRNA” samples were calculated and normalized to 1.

We performed the analyses on the maximum projection image of the raw image stacks. CellProfiler 4.0.7 is used for single-cell protein quantification (Supporting Information Figure 2a). For single-cell analyses in HeLa cells, first, Hoechst-stained nuclei were identified as primary objects. Then, the Hoechst channel, mCherry channel, and GFP channel were merged and subsequently converted to a grayscale image. Cells were identified as secondary objects on this grayscale image. Following cell segmentation, mCherry intensity and GFP intensity in each cell were measured. Finally, the ratio between GFP intensity and mCherry intensity in each cell was calculated. To remove batch effects, the average ratios between GFP intensity and mCherry intensity in all the “mock ligation” samples in different batches were calculated and normalized to 1. The assumption was that the average ratios between GFP intensity and mCherry intensity in all the “mock ligation” samples are the same. Cells that contained

similar intensities to those of control samples (transfection reagents only or untransfected cells) were considered unsuccessfully transfected and thus excluded in our analysis.

Firefly Luciferase Degron Characterization. HeLa cells were transfected with Firefly-60A or Firefly degron-60A mRNAs, using the aforementioned protocol for GFP mRNA transfection. For luciferase decay measurements, cells were grown for 24 h, then transferred to media containing 100 µg/mL of cycloheximide (CHX) to halt translation. At various time points following CHX addition, cells were lysed and luciferase activity was measured using the Promega Dual-Glo Luciferase Assay System (Promega: E2920). For luciferase-degron mRNA time course, mRNAs were generated as previously described. Then, 250 ng of Firefly-PEST mRNAs were cotransfected into HeLa cells in a 24 well-plate along with 250 ng of Renilla luciferase mRNA (E-PAP-tailed) as an internal control. Six hours after transfection, cells were reseeded into four separate opaque white-walled, clear-bottomed plates for lysis at varying time points, as specified.

For *in vitro* translation experiments, 100 ng of each Firefly-PEST mRNA was mixed with 200 ng of Renilla mRNA (E-PAP-tailed) to serve as an internal control. These were denatured at 65 °C for 5 min, placed on ice for 10 min, and added to serve as templates for a 50 µL of rabbit reticulocyte lysate reaction (Promega: L4960), assembled and incubated according to the manufacturer’s protocol. Following a 1.5 h incubation, 2 µL of each reaction was diluted in 20 µL of 1×PBS and measured using the Promega Dual-Glo assay. Three technical replicates were taken for each of three biological replicates for each condition tested.

RNA Isolation and cDNA Preparation. HeLa cells were seeded to ~75% confluence on 12-well plastic plates and transfected with mRNA using the protocol described earlier. For the preparation of positive controls, either 200 ng of poly(I:C), 500 ng of poly(I:C) (InvivoGen: tlr1-picw), or 500 ng of unmodified GFP mRNA (containing 100% replacement of N¹-methylpseudouridine with uridine and E-PAP poly(A) tailed using 100% rATP) was transfected into cells using 3 µL of Lipofectamine MessengerMax (Thermo Fisher Scientific). Following transfection and cell reseeding, cells were collected at 48 h post-transfection, media were removed, and 350 µL of Trizol was pipetted into each well for RNA storage at -80 °C. Unmodified GFP mRNA was prepared from the pCS2_hMGFP template, which did not contain a 60A template-encoded tail. Unmodified GFP mRNA contained 100% UTP instead of N¹-methylpseudouridine, and it was poly(A) tailed using E-PAP tailing.

Total RNA was extracted from Trizol-stored samples using Direct-zol RNA Miniprep Kit (Zymo Research: R2051) according to the manufacturer’s protocol. The optional DNase digestion was performed, also according to the manufacturer’s protocol. Isolated RNA was then concentrated using RNA Clean & Concentrator-5 (Zymo Research: R1013) and eluted in nuclease-free water containing 1:100 Superase-In. RNA was then quantified using Nanodrop prior to storage at -80 °C.

Reverse transcription of total RNA was performed using SuperScript IV Reverse Transcriptase (ThermoFisher Scientific: 18090200). Then, 500 ng of total RNA was mixed with 1 µL of Random Primer Mix (NEB: S1330S) and brought up to a total volume of 13 µL. This mixture was heated at 65 °C for 5 min, then immediately placed on ice during the next step of reaction assembly. The following reagents and volumes were then added to the 13 µL of annealed mixture: 4 µL of 5× SSIV reaction buffer, 1 µL (0.5 mM final) of 10 mM dNTP mix (ThermoFisher Scientific: 18427013), 1 µL of 100 mM DTT, 0.5 µL of Superase RNase-In, and 1 µL of SuperScript IV RT enzyme (200 U/µL).

Reactions were mixed, then incubated at 23 °C for 10 min, followed by incubation at 50 °C for 10 min, and terminated by incubation at 80 °C for 10 min. A portion of select cDNA reactions was saved to be used as standards for the calibration/dilution curve. However, for all samples to be quantified by RT-qPCR, 5× dilutions from these cDNA reactions were prepared by the addition of nuclease free water and stored at -80 °C prior to use.

RT-qPCR. RT-qPCR was performed in clear LightCycler 384-well plates (Roche: 04729749001), using Power SYBR Green PCR Master Mix (ThermoFisher Scientific: 4367659). Each reaction contained 1 μ L of cDNA template (previously diluted 5 \times), 500 nM each (final concentration) of the forward and reverse primers (see Supporting Information Table 1 for sequences), and 10 μ L of 2 \times Power SYBR Green Master Mix. Reaction total volumes were brought up to 20 μ L total prior to processing on a Bio-Rad CFX384 Touch Real-Time PCR Detection System. Cycling settings used for *hMGFP*, *mCherry*, and *hActb* were 95 °C for 10 min (x1); 95 °C for 10 s, 60 °C for 30 s, [Plate Read] (x40), followed by melt curve analysis (65.0 to 95.0 °C, increment 0.5 °C + [Plate Read]). For *IFNB1* qPCR, cycling settings used were 95 °C for 10 min (x1); 95 °C for 10 s, 57 °C for 15 s, 60 °C for 30 s, [Plate Read] (x40), followed by melt curve analysis (65.0 to 95.0 °C, increment 0.5 °C + [Plate Read]).

Relative mRNA quantities were calculated using the relative quantification method, which requires a standard curve. We selected “positive control” samples as our standards and performed a 2-fold dilution series to produce standard curves from which to calculate reaction efficiencies (E) for each measured gene (using linear fitting on a log–log scale). For GFP and *mCherry* quantification, we selected a cDNA stock solution corresponding to one of the biological replicates of unligated GFP-60 mRNA + *mCherry* transfections as our standard. For *IFNB1* quantification, we used one of the biological replicates for the 500 ng poly(I:C) transfection condition as our standard. For *hActb* quantification, we used cDNA from one of our “transfection conditions only” samples as our standard. To ensure all cDNA measurements of unknown samples would be within range of linearity determined by our standard curves, we diluted all cDNA stocks that were not used as standards 5 \times (as mentioned previously) prior to being measured by RT-qPCR.

Following linear fitting of our standard curves (3 \times technical replicates for each dilution), we calculated PCR reaction efficiencies (GFP, 2.05; *mCherry*, 2.24; *IFNB1*, 2.11; *hActb*, 2.09). We performed 3 \times technical replicates for each cDNA sample to be tested, and we averaged technical replicate Cq values to obtain a value corresponding to each biological replicate. To perform normalization to a specific sample (e.g., “mock ligation”), the biological replicates’ Cq values for normalization standard were averaged to give a “standard Cq”. Then, each test sample’s Cq values were subtracted from this “standard Cq” to give a dCq value. Reaction efficiencies (E) were raised to the power of these dCq values to give individual “fold changes” for each biological test sample. To normalize GFP by both *mCherry* and *hActb*, the geometric mean was taken of *mCherry* and *hActb* “fold changes” that were calculated previously. The GFP “fold changes” were then divided by these normalization factors to produce the final values used for quantification of GFP (Figure 2c, Supporting Information Table 3). For the normalization of *IFNB1*, *hActb* values for each sample were used directly (without the geometric mean calculation; Supporting Information Table 3). Data points shown in each graph correspond to the averages of three technical replicates performed for every biologically replicate. Negative controls (e.g., N.T.C. and transfection only) for specific conditions were omitted from calculations, when they did not produce a Cq value.

mRNA Quantification in Transfected Cell Culture Using STARmap. We measured *mCherry* and *GFP* mRNA quantities in transfected cells using STARmap,²⁸ an imaging-based method that reads out individual mRNA molecules as a barcoded DNA colony. We followed the STARmap procedure for cell cultures as published.²⁸ Briefly, following fluorescent protein imaging, the cells were fixed with 1.6% PFA (Electron Microscope Sciences, 15710-S)/1XPBS (Gibco, 10010-023) at RT for 10 min before further fixation and permeabilization with prechilled methanol at –20 °C (up to 1 week). Subsequently, the methanol was removed, and the cells were rehydrated with PBSTR/Glycine/YtRNA (PBS with 0.1%Tween-20 [TEKNOVA INC, 100216-360], 0.5% SUPERaseIn [Invitrogen, AM2696], 100 mM glycine, 1% yeast tRNA) at RT for 15 min followed by one PBSTR wash. The samples were then hybridized with SNAI1 probes targeting *mCherry* and *GFP* mRNA sequences in the hybridization buffer (2XSSC [Sigma-Aldrich, S6639], 10% formamide

[Calbiochem, 655206], 1% Tween-20, 20 mM RVC [ribonucleoside vanadyl complex, New England Biolabs, S1402S], 0.5% SUPERaseIn, and 1% yeast tRNA, 100 nM each probe) at 40 °C overnight (see Supporting Information Table 1 for “SNAI1 probe” sequences). The cells were then washed with PBSTR twice at 37 °C (20 min each wash) and high salt wash buffer (PBSTR with 4XSSC) once at 37 °C before rinsing once with PBSTR at RT. A ligation reaction was performed for 2 h at RT to circularize padlock probes that were adjacent to a primer. After two washes with PBSTR, rolling circle amplification was initiated from the primer using Phi29 (ThermoFisher, EP0094) at 30 °C for 2 h with amino-dUTP (Invitrogen, AM8439) spiked in. After two more washes with PBSTR, the DNA amplicons were modified to be polymerizable by 20 mM MA-NHS (Sigma-Aldrich, 730300-1G) in PBST buffer at RT for 2 h. The samples were then converted into a hydrogel-cell hybrid before proteinase K (Invitrogen, 25530049) clearing of fluorescent proteins at RT overnight. The samples were washed three times with PBST before being stained with fluorescent detection oligo in the wash and imaging buffer (2XSSC, 10% formamide) at 37 °C for 1 h (see Supporting Information Table 1 for “fluorescent detection probe” sequences). Finally, the samples were washed three times with the wash and imaging buffer at RT and stained with DAPI before imaging in the wash and imaging buffer. Confocal imaging stacks were taken with a Leica Stellaris 8 or SP8 with a 40 \times oil objective at a pixel size of 283 × 283 nm. A 14- μ m stack is imaged with 1 μ m/step × 15 steps. Four representative fields of view are taken for each well, one from each quadrant. The same imaging setting was used for all the samples to be compared. Excitation/detection wavelengths are as follows: DAPI, Diode 405 nm/~/[420–489] nm; Alexa546, WLL 557 nm/~/[569–612] nm; Alexa647, WLL 653 nm/~/[668–738] nm.

MATLAB 2021a and CellProfiler 4.0.7 were used for the amplicon count-based STARmap fluorescence image analysis (Supporting Information Figure 2c). First, the centroids of amplicons in each fluorescent channel (GFP, *mCherry*) were identified by finding extended maxima on images. Then a 3 × 3 × 3 voxel volume centering the centroid of each fluorescent dot was defined. Within each voxel volume, the integrated intensities in the *mCherry* and GFP channels were calculated, and the ratio between *mCherry* intensity and GFP intensity was used for amplicon classification. After these measurements had been performed on all of the images in a batch, all of the measurements were pooled together, and the distribution of log(*mCherry*/GFP) values was plotted. The corresponding ratio values at the nadirs (local minimum) on the distribution plot were identified as cutoff values. The first cutoff value less than 0 was noted as *cutoff1*, and the first cutoff value greater than 0 was noted as *cutoff2*. Any amplicon with a log(*mCherry*/GFP) value smaller than *cutoff1* was identified as a *GFP* amplicon. Any amplicon with a log(*mCherry*/GFP) value larger than *cutoff2* was identified as a *mCherry* amplicon. Any amplicon with a log(*mCherry*/GFP) value between *cutoff1* and *cutoff2* was identified as a granule. Amplicon classification information, as well as the location of every amplicon, was saved in a file. In bulk STARmap quantification, in each figure, the ratio between the number of *GFP* amplicons and the number of *mCherry* amplicons was calculated and used to reflect the amount of *GFP* mRNAs. In single-cell STARmap quantification, cell segmentation was performed using the same method as cell segmentation in single-cell protein quantification, and the segmentation masks were saved as uint16 images. We then assigned amplicons to cells according to where they were located on the masks. The ratio between the number of *GFP* amplicons and the number of *mCherry* amplicons in each cell was calculated and used to reflect the amount of *GFP* mRNAs in a single cell. Cells with no *GFP* amplicons or no *mCherry* amplicons were considered unsuccessfully transfected and thus excluded from our analyses.

ASSOCIATED CONTENT

Supporting Information

The Supporting Information is available free of charge at <https://pubs.acs.org/doi/10.1021/acschembio.1c00569>.

Supplemental figures include representative RNase H characterization of mocRNAs, additional single-HeLa cell quantification of mocRNA expression, and fluorescence data from the screening of modified nucleotides for E-PAP poly(A) tail modification; further expression data from length-controlled G4 oligonucleotides and mocRNA toxicity profiling in HeLa and primary rat cortical neurons; supplemental tables include additional oligonucleotide sequences used in this study, as well as statistics from Figure 2a,c and Figure 5a,b (PDF)

AUTHOR INFORMATION

Corresponding Author

Xiao Wang – *Broad Institute of MIT and Harvard, Cambridge, Massachusetts 02142, United States; Department of Chemistry, Massachusetts Institute of Technology, Cambridge, Massachusetts 02139, United States; Stanley Center for Psychiatric Research, Broad Institute of MIT and Harvard, Cambridge, Massachusetts 02142, United States;*  [0000-0002-3090-9894](https://orcid.org/0000-0002-3090-9894); Email: xwangx@mit.edu

Authors

Abhishek Aditham – *Broad Institute of MIT and Harvard, Cambridge, Massachusetts 02142, United States; Department of Biological Engineering, Massachusetts Institute of Technology, Cambridge, Massachusetts 02142, United States;*  [0000-0003-3203-4574](https://orcid.org/0000-0003-3203-4574)

Hailing Shi – *Broad Institute of MIT and Harvard, Cambridge, Massachusetts 02142, United States; Department of Chemistry, Massachusetts Institute of Technology, Cambridge, Massachusetts 02139, United States;*  [0000-0001-7355-378X](https://orcid.org/0000-0001-7355-378X)

Jianting Guo – *Broad Institute of MIT and Harvard, Cambridge, Massachusetts 02142, United States; Department of Chemistry, Massachusetts Institute of Technology, Cambridge, Massachusetts 02139, United States;*  [0000-0002-5691-5707](https://orcid.org/0000-0002-5691-5707)

Hu Zeng – *Broad Institute of MIT and Harvard, Cambridge, Massachusetts 02142, United States;*  [0000-0003-4773-205X](https://orcid.org/0000-0003-4773-205X)

Yiming Zhou – *Broad Institute of MIT and Harvard, Cambridge, Massachusetts 02142, United States;*  [0000-0002-8365-0396](https://orcid.org/0000-0002-8365-0396)

Sarah Dunn Wade – *Broad Institute of MIT and Harvard, Cambridge, Massachusetts 02142, United States; Stanley Center for Psychiatric Research, Broad Institute of MIT and Harvard, Cambridge, Massachusetts 02142, United States; Department of Neuroscience, University of California San Francisco, San Francisco, California 94158, United States;*  [0000-0002-5746-5111](https://orcid.org/0000-0002-5746-5111)

Jiahao Huang – *Broad Institute of MIT and Harvard, Cambridge, Massachusetts 02142, United States;*  [0000-0002-6349-9799](https://orcid.org/0000-0002-6349-9799)

Jia Liu – *John A. Paulson School of Engineering and Applied Sciences, Harvard University, Cambridge, Massachusetts 02134, United States;*  [0000-0003-2217-6982](https://orcid.org/0000-0003-2217-6982)

Complete contact information is available at:

<https://pubs.acs.org/10.1021/acschembio.1c00569>

Author Contributions

A.A., H.S., and X.W. conceived the idea and designed experiments. A.A. and H.S. performed wet lab experiments and data acquisition. A.A., H.S., and J.G. performed data analysis. Y.Z. and H.Z. contributed to confocal imaging experiments. S.W. provided primary neurons and guidance on neuronal cultures. J.H. provided computational support and verification of single-cell fluorescence and RNA quantification. H.Z. aided with protocol optimization for STARmap imaging. A.A., H.S., J.G., J.L., and X.W. wrote and revised the manuscript. X.W. supervised the study.

Author Contributions

▽ These authors contributed equally.

Notes

The authors declare the following competing financial interest(s): A patent application has been filed relating to this work.

ACKNOWLEDGMENTS

H. Shi is supported by the Helen Hay Whitney Postdoc Fellowship. We would like to thank other members of X. Wang's lab for helpful feedback during data collection and writing our manuscript. We would also like to thank M. Sheng at the Broad Institute for supplying primary rat cortical neurons for our mRNA expression experiments and S. Schreiber at the Broad Institute for input on the manuscript. X. Wang acknowledges support from the Searle Scholars Program, Ono Pharma Breakthrough Initiative Award, Thomas D. and Virginia W. Cabot Professorship, and the Edward Scolnick Professorship. Raw imaging and STARmap data supporting the findings of this study are available from the corresponding author upon request. All customized scripts are listed and available on GitHub (https://github.com/wanglab-broad/rna_therapeutic).

REFERENCES

- (1) Polack, F. P.; Thomas, S. J.; Kitchin, N.; Absalon, J.; Gurtman, A.; Lockhart, S.; Perez, J. L.; Perez Marc, G.; Moreira, E. D.; Zerbini, C.; Bailey, R.; Swanson, K. A.; Roychoudhury, S.; Koury, K.; Li, P.; Kalina, W. V.; Cooper, D.; Frenck, R. W.; Hammitt, L. L.; Türeci, O.; Nell, H.; Schaefer, A.; Unal, S.; Tresnan, D. B.; Mather, S.; Dormitzer, P. R.; Sahin, U.; Jansen, K. U.; Gruber, W. C. Safety and Efficacy of the BNT162b2 mRNA Covid-19 Vaccine. *N. Engl. J. Med.* **2020**, *383*, 2603–2615.
- (2) Lombardi, A.; Bozzi, G.; Ungaro, R.; Villa, S.; Castelli, V.; Mangioni, D.; Muscatello, A.; Gori, A.; Bandera, A. Mini Review Immunological Consequences of Immunization With COVID-19 mRNA Vaccines: Preliminary Results. *Front. Immunol.* **2021**, *12*, 657711.
- (3) Sahin, U.; Karikó, K.; Türeci, Ö mRNA-based therapeutics—developing a new class of drugs. *Nat. Rev. Drug Discovery* **2014**, *13*, 759–780.
- (4) Dammes, N.; Peer, D. Paving the Road for RNA Therapeutics. *Trends Pharmacol. Sci.* **2020**, *41*, 755–775.
- (5) Weng, Y.; Li, C.; Yang, T.; Hu, B.; Zhang, M.; Guo, S.; Xiao, H.; Liang, X. J.; Huang, Y. The challenge and prospect of mRNA therapeutics landscape. *Biotechnol. Adv.* **2020**, *40*, 107534.
- (6) Petsch, B.; Schnee, M.; Vogel, A. B.; Lange, E.; Hoffmann, B.; Voss, D.; Schlake, T.; Thess, A.; Kallen, K. J.; Stitz, L.; et al. Protective efficacy of in vitro synthesized, specific mRNA vaccines against influenza A virus infection. *Nat. Biotechnol.* **2012**, *30*, 1210–1216.
- (7) Richner, J. M.; Jagger, B. W.; Shan, C.; Fontes, C. R.; Dowd, K. A.; Cao, B.; Himansu, S.; Caine, E. A.; Nunes, B. T. D.; Medeiros, D. B. A.; et al. Vaccine Mediated Protection Against Zika Virus-Induced Congenital Disease. *Cell* **2017**, *170*, 273–283.

- (8) Tai, W.; Zhang, X.; Drelich, A.; Shi, J.; Hsu, J. C.; Luchsinger, L.; Hillyer, C. D.; Tseng, C. T. K.; Jiang, S.; Du, L. A novel receptor-binding domain (RBD)-based mRNA vaccine against SARS-CoV-2. *Cell Res.* **2020**, *30*, 932–935.
- (9) Chen, C.; Ezzeddine, N.; Shyu, A. Messenger RNA half-life measurements in mammalian cells. *Methods Enzymol.* **2008**, *448*, 335–357.
- (10) Karikó, K.; Muramatsu, H.; Welsh, F. A.; Ludwig, J.; Kato, H.; Akira, S.; Weissman, D. Incorporation of pseudouridine into mRNA yields superior nonimmunogenic vector with increased translational capacity and biological stability. *Mol. Ther.* **2008**, *16*, 1833–1840.
- (11) Karikó, K.; Buckstein, M.; Ni, H.; Weissman, D. Suppression of RNA recognition by Toll-like receptors: the impact of nucleoside modification and the evolutionary origin of RNA. *Immunity* **2005**, *23*, 165–175.
- (12) Andries, O.; McCafferty, S.; De Smedt, S. C.; Weiss, R.; Sanders, N. N.; Kitada, T. N¹-methylpseudouridine-incorporated mRNA outperforms pseudouridine-incorporated mRNA by providing enhanced protein expression and reduced immunogenicity in mammalian cell lines and mice. *J. Controlled Release* **2015**, *217*, 337–344.
- (13) Kormann, M. S.; Hasenpusch, G.; Aneja, M. K.; Nica, G.; Flemmer, A. W.; Herber-Jonat, S.; Huppmann, M.; Mays, L. E.; Illenyi, M.; Schams, A.; et al. Expression of therapeutic proteins after delivery of chemically modified mRNA in mice. *Nat. Biotechnol.* **2011**, *29*, 154–157.
- (14) Li, B.; Luo, X.; Dong, Y. Effects of Chemically Modified Messenger RNA on Protein Expression. *Bioconjugate Chem.* **2016**, *27*, 849–853.
- (15) Aurup, H.; Siebert, A.; Benseler, F.; Williams, D.; Eckstein, F. Translation of 2'-modified mRNA in vitro and in vivo. *Nucleic Acids Res.* **1994**, *22*, 4963–4968.
- (16) Choi, J.; Indrisiunaite, G.; DeMirci, H.; Ieong, K. W.; Wang, J.; Petrov, A.; Prabhakar, A.; Rechavi, G.; Dominissini, D.; He, C.; et al. 2'-O-methylation in mRNA disrupts tRNA decoding during translation elongation. *Nat. Struct. Mol. Biol.* **2018**, *25*, 208–216.
- (17) Anhäuser, L.; Hüwel, S.; Zobel, T.; Rentmeister, A. Multiple covalent fluorescence labeling of eukaryotic mRNA at the poly(A) tail enhances translation and can be performed in living cells. *Nucleic Acids Res.* **2019**, *47*, No. e42.
- (18) Strzelecka, D.; Smietanski, M.; Sikorski, P. J.; Warminski, M.; Kowalska, J.; Jemielity, J. Phosphodiester modifications in mRNA poly(A) tail prevent deadenylation without compromising protein expression. *RNA* **2020**, *26*, 1815–1837.
- (19) Łabno, A.; Tomecki, R.; Dziembowski, A. Cytoplasmic RNA decay pathways - Enzymes and mechanisms. *Biochim. Biophys. Acta, Mol. Cell Res.* **2016**, *1863*, 3125–3147.
- (20) Garneau, N. L.; Wilusz, J.; Wilusz, C. J. The highways and byways of mRNA decay. *Nat. Rev. Mol. Cell Biol.* **2007**, *8*, 113–126.
- (21) Eckstein, F. Phosphorothioates, essential components of therapeutic oligonucleotides. *Nucleic Acid Ther.* **2014**, *24*, 374–387.
- (22) Stowell, J. A.; Webster, M. W.; Kögel, A.; Wolf, J.; Shelley, K. L.; Passmore, L. A. Reconstitution of Targeted Deadenylation by the Ccr4-Not Complex and the YTH Domain Protein Mmi1. *Cell Rep.* **2016**, *17*, 1978–1989.
- (23) Yang, Y.; Lindahl, T.; Barnes, D. Trex1 exonuclease degrades ssDNA to prevent chronic checkpoint activation and autoimmune disease. *Cell* **2007**, *131*, 873–886.
- (24) Takahashi, A.; Loo, T. M.; Okada, R.; Kamachi, F.; Watanabe, Y.; Wakita, M.; Watanabe, S.; Kawamoto, S.; Miyata, K.; Barber, G. N.; Ohtani, N.; Hara, E. Downregulation of cytoplasmic DNases is implicated in cytoplasmic DNA accumulation and SASP in senescent cells. *Nat. Commun.* **2018**, *9*, 1249.
- (25) Chen, J.; Chiang, Y.; Denis, C. CCR4, a 3'-5' poly(A) RNA and ssDNA exonuclease, is the catalytic component of the cytoplasmic deadenylase. *EMBO J.* **2002**, *21*, 1414–1426.
- (26) Cerritelli, S.; Crouch, R. Ribonuclease H: the enzymes in eukaryotes. *FEBS J.* **2009**, *276*, 1494–1505.
- (27) Leonhardt, C.; Schwake, G.; Stögbauer, T. R.; Rappl, S.; Kuhr, J. T.; Ligon, T. S.; Rädler, J. O. Single-cell mRNA transfection studies: delivery, kinetics and statistics by numbers. *Nanomedicine* **2014**, *10*, 679–688.
- (28) Wang, X.; Allen, W. E.; Wright, M. A.; Sylwestrak, E. L.; Samusik, N.; Vesuna, S.; Evans, K.; Liu, C.; Ramakrishnan, C.; Liu, J.; Nolan, G. P.; Bava, F.-A.; Deisseroth, K. Three-dimensional intact-tissue sequencing of single-cell transcriptional states. *Science* **2018**, *361*, No. eaat5691.
- (29) Li, X.; Zhao, X.; Fang, Y.; Jiang, X.; Duong, T.; Fan, C.; Huang, C. C.; Kain, S. R. Generation of destabilized green fluorescent protein as a transcription reporter. *J. Biol. Chem.* **1998**, *273*, 34970–34975.
- (30) Lin, C. Y.; Perche, F.; Ikegami, M.; Uchida, S.; Kataoka, K.; Itaka, K. Messenger RNA-based therapeutics for brain diseases: An animal study for augmenting clearance of beta-amyloid by intracerebral administration of neprilysin mRNA loaded in polyplex nanomicelles. *J. Controlled Release* **2016**, *235*, 268–275.
- (31) Williams, D. J.; Puhl, H. L.; Ikeda, S. R. A simple, highly efficient method for heterologous expression in mammalian primary neurons using cationic lipid-mediated mRNA transfection. *Frontiers in Neuroscience* **2010**, *4*, 181.
- (32) Inguscio, S.; Verlengia, G.; Soukupova, M.; Zucchini, S.; Simonato, M. Gene therapy tools for brain diseases. *Frontiers in Pharmacology* **2019**, *10*, 724.
- (33) Honda, K.; Yanai, H.; Takaoka, A.; Taniguchi, T. Regulation of the type I IFN induction: a current view. *Int. Immunol.* **2005**, *17*, 1367–1378.
- (34) Wienert, B.; Shin, J.; Zelin, E.; Pestal, K.; Corn, J. E. In vitro-transcribed guide RNAs trigger an innate immune response via the RIG-I pathway. *PLoS Biol.* **2018**, *16*, No. e2005840.
- (35) Linehan, M. M.; Dickey, T. H.; Molinari, E. S.; Fitzgerald, M. E.; Potapova, O.; Iwasaki, A.; Pyle, A. M. A minimal RNA ligand for potent RIG-I activation in living mice. *Science Advances* **2018**, *4*, No. e1701854.
- (36) Hausmann, S.; Marq, J. B.; Tapparel, C.; Kolakofsky, D.; Garcin, D. RIG-I and dsRNA-induced IFN β activation. *PLoS One* **2008**, *3*, No. e3965.
- (37) Cao, Z.; Huang, C. C.; Tan, W. Nuclease resistance of telomere-like oligonucleotides monitored in live cells by fluorescence anisotropy imaging. *Anal. Chem.* **2006**, *78*, 1478–1484.
- (38) Barragán-Iglesias, P.; Lou, T. F.; Bhat, V. D.; Megat, S.; Burton, M. D.; Price, T. J.; Campbell, Z. T. Inhibition of Poly (A)-binding protein with a synthetic RNA mimic reduces pain sensitization in mice. *Nat. Commun.* **2018**, *9*, 1–17.
- (39) Rydzik, A. M.; Warminski, M.; Sikorski, P. J.; Baranowski, M. R.; Walczak, S.; Kowalska, J.; Zuberek, J.; Lukaszewicz, M.; Nowak, E.; W. Claridge, T. D.; Darzynkiewicz, E.; Nowotny, M.; Jemielity, J.; et al. mRNA cap analogues substituted in the tetraphosphate chain with CX2: identification of O-to-CCl₂ as the first bridging modification that confers resistance to decapping without impairing translation. *Nucleic Acids Res.* **2017**, *45*, 8661–8675.
- (40) Strenkowska, M.; Kowalska, J.; Lukaszewicz, M.; Zuberek, J.; Su, W.; Rhoads, R. E.; Darzynkiewicz, E.; Jemielity, J. Towards mRNA with superior translational activity: synthesis and properties of ARCA tetraphosphates with single phosphorothioate modifications. *New J. Chem.* **2010**, *34*, 993–1007.
- (41) Kawaguchi, D.; Kodama, A.; Abe, N.; Takeuchi, K.; Hashiya, F.; Tomoike, F.; Nakamoto, K.; Kimura, Y.; Shimizu, Y.; Abe, H. Phosphorothioate Modification of mRNA Accelerates the Rate of Translation Initiation to Provide More Efficient Protein Synthesis. *Angew. Chem., Int. Ed.* **2020**, *59*, 17403–17407.
- (42) Boo, S.; Kim, Y. The emerging role of RNA modifications in the regulation of mRNA stability. *Exp. Mol. Med.* **2020**, *52*, 400–408.
- (43) Zhao, B. S.; Wang, X.; Beadell, A. V.; Lu, Z.; Shi, H.; Kuuspalu, A.; Ho, R. K.; He, C. m⁶A-dependent maternal mRNA clearance facilitates zebrafish maternal-to-zygotic transition. *Nature* **2017**, *542*, 475–478.
- (44) Carpenter, A. E.; Jones, T. R.; Lamprecht, M. R.; Clarke, C.; Kang, I.; Friman, O.; Guertin, D. A.; Chang, J.; Lindquist, R. A;

Moffat, J.; Golland, P.; Sabatini, D. M. CellProfiler: image analysis software for identifying and quantifying cell phenotypes. *Genome biology* 2006, 7, R100.

□ Recommended by ACS

Functional Comparison between Endogenous and Synthetic Notch Systems

Bassma Khamaisi, David Sprinzak, et al.
SEPTEMBER 15, 2022
ACS SYNTHETIC BIOLOGY

READ

Ribosome Stalling of N-Linked Glycoproteins in Cell-Free Extracts

Sean S. Chung, Matthew P. DeLisa, et al.
NOVEMBER 18, 2022
ACS SYNTHETIC BIOLOGY

READ

Method for Identifying Sequence Motifs in Pre-miRNAs for Small-Molecule Binding

Yusuke Takashima, Kazuhiko Nakatani, et al.
SEPTEMBER 23, 2022
ACS CHEMICAL BIOLOGY

READ

Site-Selective Tyrosine Phosphorylation in the Activation of the p50 Subunit of NF-κB for DNA Binding and Transcription

Shengxi Chen, Sidney M. Hecht, et al.
DECEMBER 19, 2022
ACS CHEMICAL BIOLOGY

READ

[Get More Suggestions >](#)